fluids

MDPI

Article

Demonstrating the Kelvin-Helmholtz Instability Using a Low-Cost Experimental Apparatus and Computational Fluid Dynamics Simulations

Melissa M. Gibbons *, Dillon Muldoon and Imane Khalil

Department of Mechanical Engineering, University of San Diego, San Diego, CA 92110, USA; dmuldoon@sandiego.edu (D.M.); ikhalil@sandiego.edu (I.K.)
* Correspondence: mgibbons@sandiego.edu

Abstract: A Kelvin-Helmholtz instability is formed when two fluids of different densities exert a shear on one another at their interface when flowing in opposite directions. This paper presents a step-by-step guide for the design of a low-cost, small-scale, experimental tilt tube apparatus and a corresponding computational fluid dynamics (CFD) model that can be used to introduce the Kelvin-Helmholtz instability to undergraduate mechanical engineering students in several courses. A thermal-fluids laboratory course is taken by our fourth-year mechanical engineering students, and the overall variety of experiments has been limited by the cost of commercial teaching equipment. The tilt tube apparatus allows students to induce and record the Kelvin-Helmholtz instability, and no ongoing costs are involved in incorporating this experiment into the course. In our introductory CFD course, students perform CFD simulations as part of the design and analysis process. Developing a two-dimensional (2D) CFD model with two different fluids is well within their capabilities after completing initial software and simulation tutorial exercises and homework. Representative experiments were conducted with fresh water and salt water of different densities, and results showed that both the amplitude of the waves and the amount of time the instability was visible decreased with increasing salt water salinity. Results from a 2D CFD model developed in Ansys Fluent exhibited the same trends as the experimental data.

Keywords: fluid mechanics; CFD; Kelvin-Helmholtz; tilt tube experiment; fluid instability

check for updates

Citation: Gibbons, M.M.; Muldoon, D.; Khalil, I. Demonstrating the Kelvin-Helmholtz Instability Using a Low-Cost Experimental Apparatus and Computational Fluid Dynamics Simulations. *Fluids* **2023**, *8*, 318. https://doi.org/10.3390/fluids8120318

Academic Editors: Tim Persoons and D. Andrew S. Rees

Received: 10 November 2023
Revised: 7 December 2023
Accepted: 9 December 2023
Published: 12 December 2023

1. Introduction

On a conceptually basic level, a Kelvin-Helmholtz instability is formed when two fluids of slightly different densities exert a shear on one another at their interface when flowing in opposite directions in a way that can be described as parallel to the interface [1–3]. This counterflow eventually causes the interface to enter the turbulent region of flow, and the instability proceeds to grow and permanently departs from the initial unperturbed condition. The smooth, wavelike oscillations that are produced grow in amplitude until the wave crests overturn [4]. Mixing between the two fluids occurs until the density is relatively uniform and the initial momentum imparted to the fluids has ceased. Kelvin-Helmholtz instabilities in the atmosphere [5] and ocean [6] are the most commonly observed examples, and documentation of the phenomenon in clouds often makes its way to traditional media [7]. This paper presents a step-by-step guide for the design and implementation of a low-cost, small-scale experimental tilt tube apparatus and the development of a corresponding computational fluid dynamics (CFD) model that can be used to introduce the Kelvin-Helmholtz instability to students in several courses in the undergraduate mechanical engineering curriculum.

The thermal-fluids laboratory is a required course for fourth-year mechanical engineering students at our university and is offered in the fall semester. The experiments that the students perform demonstrate basic heat transfer and fluid mechanics concepts. The overall variety of experiments has been limited by the high cost of commercial teaching equipment. We were inspired by several studies that focused on the design and fabrication of low-cost hardware that can be used in thermal-fluid laboratory experiments, as an alternative to purchasing expensive educational equipment [8–11]. Low-cost custom equipment has been used to demonstrate a wide variety of concepts including heat conduction (axial, radial, and fin) [10], compressible flow [8], and vapor compression refrigeration cycles [11]. Particle image velocimetry has been used to visually represent stagnation flow around a flat plate, which allowed students to quantitatively analyze video data and compare the experimental results to predicted velocity fields using potential flow theory [9]. Following a similar methodology, a low-cost tilt tube apparatus was built to demonstrate the Kelvin-Helmholtz instability. This experiment augments the other fluid experiments currently conducted by students in the course, which are simple applications of the Bernoulli equation (e.g., losses in bends and flow measurement techniques) that do not incorporate video recordings of dynamic fluid responses. Students are responsible for properly preparing the apparatus, ensuring the fluid densities are correct, recording video of the experiments, and post-processing the recorded data to determine the number and quality of the waves that develop in each experiment.

While the mathematical derivations required to describe the theoretical underpinnings of the instability are likely too advanced for an undergraduate fluid mechanics course, the phenomenon can be fairly easily simulated with CFD software. With the proliferation of affordable and validated simulation software programs, undergraduate classes in CFD and finite element analysis (FEA) have become common in the undergraduate curriculum. These courses provide an opportunity for students to apply theory to realistic problems and design projects [12] and to experience the benefits of project-based learning [13]. CFD models need to be validated using realistic data, and students should be expected to validate their models as part of the coursework; for example, CFD simulations of turbulent flow through an orifice meter were validated against published experimental data [14], and CFD simulations of stagnation flow were validated against theoretical predictions [9]. In the introductory CFD course offered as an elective by the mechanical engineering program at our university, students learn to perform CFD simulations as part of the design and analysis process with the free student version of Ansys Fluent [15]. Because fluid mechanics is a prerequisite for the course, the CFD course is typically taken by fourth-year students. This means the CFD course is either taken concurrently with or after completing the thermal-fluids laboratory course. Developing a two-dimensional (2D) CFD model with two different fluid types is well within their capabilities after completing initial software and simulation tutorial exercises and homework. Initial experimental results recorded for this study were used to preliminarily validate the CFD model, and are provided to the students so that they can be introduced to the validation process as well. Formal validation of the CFD model is proposed as future work.

2. Materials and Methods

2.1. Theoretical Framework

The occurrence of a Kelvin-Helmholtz instability depends on several factors. First and foremost are the density and viscosity of each fluid, which must be different, albeit close in numerical value. Additionally, opposing velocities at the interface are crucial to ensure a Kelvin-Helmholtz instability can form. Figure 1 is a schematic of the instability occurring at the interface between two fluids with velocities u_1 and u_2 and densities ρ_1 and ρ_2. The conservation of mass and momentum equations that dominate the flow are given in Equations (1) and (2), respectively, where U is the velocity vector field, ρ is the fluid density, μ is the dynamic viscosity, P is the pressure, and g is the gravitational acceleration vector:

$$\frac{\partial \rho}{\partial t} + \nabla \cdot (\rho U) = 0, \tag{1}$$

$$\rho\frac{dU}{dt} = -\nabla P + \mu\nabla^2 U + \rho g. \quad (2)$$

The equation for the interface perturbation, $h(x, t)$, describes how the shape of the interface evolves over time due to the velocity difference between the two fluids:

$$\frac{\partial h}{\partial t} = (u_1 - u_2)\frac{\partial h}{\partial x}. \quad (3)$$

In Equation (3), u_1 and u_2 are crucial in driving the instability. The density difference between the two fluids is indirectly considered through the velocity difference but not explicitly included in the equation for the displacement. A visual representation of the Kelvin-Helmholtz instability is shown in Figure 1.

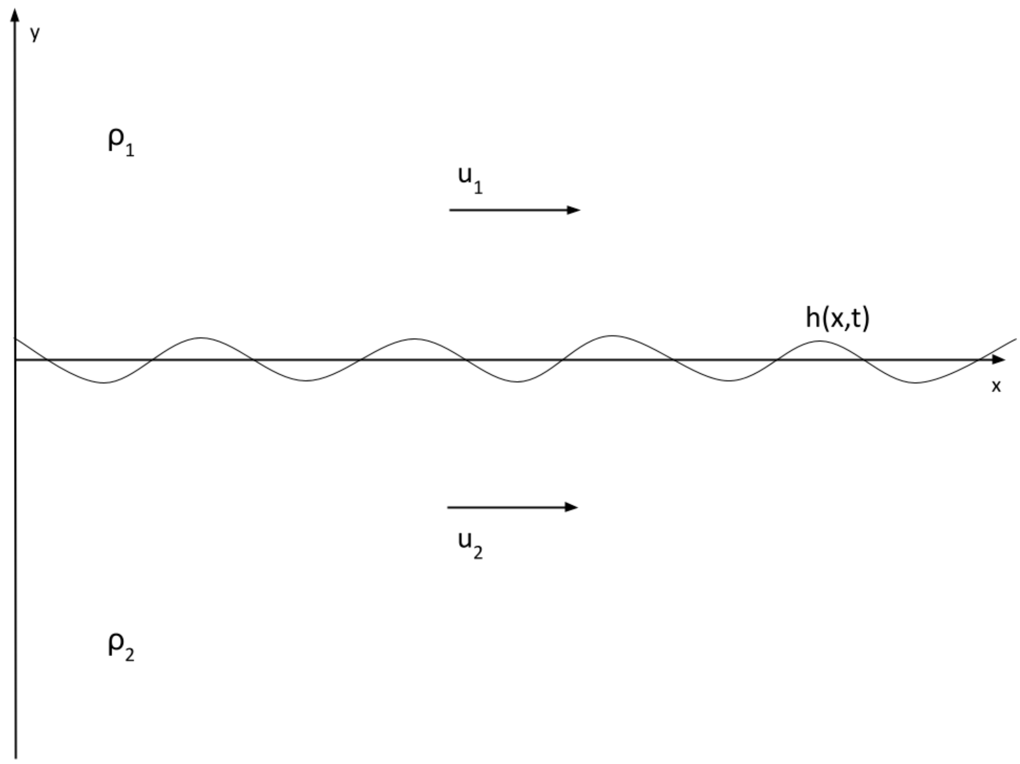

Figure 1. Schematic of the Kelvin-Helmholtz instability.

2.2. Experimental Apparatus

A low-cost tilt tube was designed and fabricated to demonstrate the Kelvin-Helmholtz instability in a laboratory setting. Requirements for the apparatus included: a high visibility of the fluids inside the tube, the ability for the instability to form with the least amount of disturbance, a rigid yet crack-resistant structure, and a design that was easy to manufacture, assemble, maintain, and transport. The tilt tube was constructed with acrylic because it is clear, rigid, relatively sturdy in the event of a light impact, and corrosion-resistant so that it may be continually reused. Additionally, acrylic is easy to repair compared with other suitable materials, such as glass.

During the initial design phase, circular and rectangular tube cross-sections were considered. Because of the possibility of unwanted flow perturbations and the need for a custom support, a cylindrical tube was ruled out as a possibility. In contrast, the rectangular tube was relatively easy to fabricate, could be quickly mounted on readily available tilting stands, and produced stable, approximately 2D flow. The rectangular tilt tube was designed in the SOLIDWORKS 2023 CAD software package (version 16000) [16] and is shown in Figure 2. The outer dimensions of the tube are 0.2023 m high, 0.0508 m wide, and 1.8034 m long. The inner dimensions of the tube are 0.1524 m high, 0.0381 m wide, and 1.7653 m long. The six individual acrylic pieces were glued together with an acrylic epoxy and clamped together until the epoxy was cured. The base of the tilt tube (0.0381 m) was thicker than the top (0.0127 m) to allow mounting holes to be drilled into the base without compromising the integrity of the acrylic and to prevent bowing under consistent static loading. Additionally, it was necessary to account for the clearance needed to mount the tilt tube to a stand so that the entirety of the interior of the tube remained visible upon use. To minimize the cost and time needed to construct the finished product, the acrylic tilt tube was mounted to a low-cost commercially available Triton multi-stand. When mounted to the stand, the tube was able to tilt to over 60° before touching the ground, and the tilt angle was limited only by the tube's length. The incorporation of this stand also made transportation of the assembly much easier.

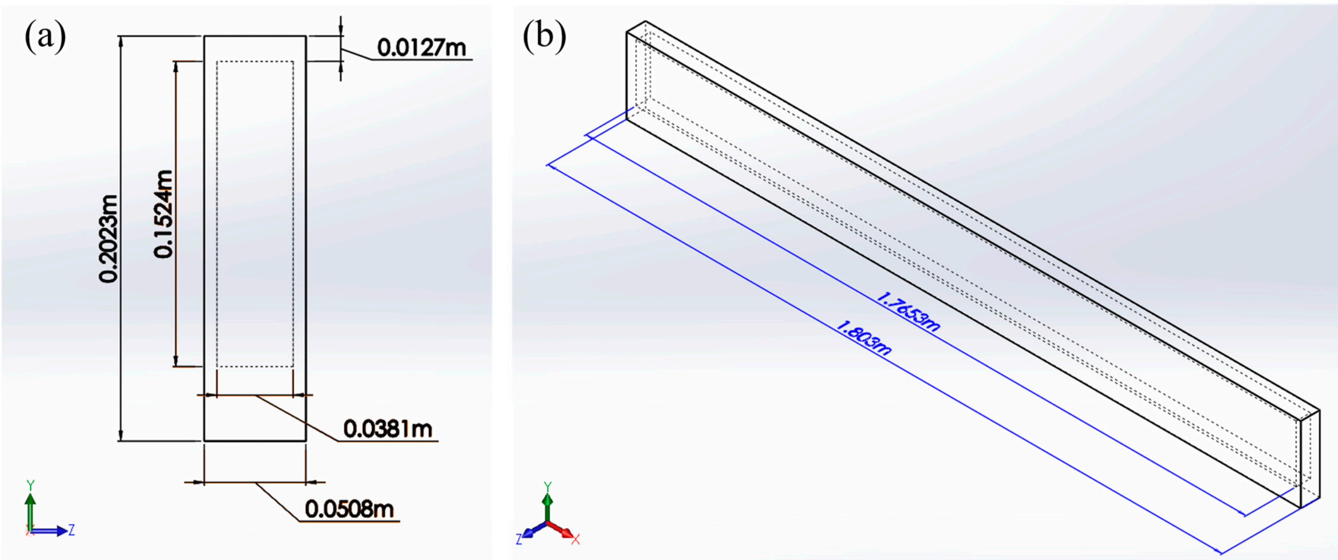

Figure 2. CAD model of the tilt tube created in SOLIDWORKS. (**a**) Cross-sectional view and (**b**) isometric view, where all dimensions are shown in meters.

2.3. Experimental Procedure

Prior to running the physical experiments, several precautions were taken to ensure the tilt tube apparatus was functioning properly. The apparatus was checked for any cracks or deformations, particularly around the end caps, which were attached with cement. The tube was rinsed with fresh water before and after each trial to prevent the formation of salt crystals inside the tube.

Samples of fresh water and salt water were then created; these fluids were chosen since the Kelvin-Helmholtz instability is best viewed when the densities of the two fluids are close to each other. Tap water was used to prepare both mixtures because of its immediate availability in the laboratory. Both liquid samples were prepared by filling a cylindrical container with 10 L (0.01 m^3) of tap water. To create the salt water sample, iodized salt was then added to the container and the liquid was thoroughly mixed until all salt crystals were dissolved. Fresh and salt water densities and the resulting salinity of the salt water for each trial are given in Table 1. Tracer dyes of contrasting colors were added to each mixture so they would be easy to differentiate and to make the instability visible. Food coloring can be used, but for vibrant colors that produce substantial contrast that makes the video analysis easier, dye tablets used to detect leaks in water lines are the better choice.

Table 1. Experimental properties of the liquid samples.

Trial	Water Volume (m^3)	Fresh Water Density (kg/m^3)	Fresh Water Viscosity (kg/m^s)	Salt Added (kg)	Salt Water Density (kg/m^3)	Salinity (%)	Salt Water Viscosity (kg/m^s)
1	0.01	998.2	0.001003	0.810	1079.2	7.5	0.0012
2	0.01	998.2	0.001003	1.297	1127.9	11.5	0.001375
3	0.01	998.2	0.001003	1.831	1181.3	15.5	0.00158
4	0.01	998.2	0.001003	2.417	1239.9	19.5	0.0018

The mixtures were then pumped into the apparatus. A submersible pump was placed inside the fresh water mixture first, and flexible plastic tubing was fitted onto the pump. The other end of the plastic tubing was attached to a valve system built into the apparatus itself. The valve was initially in the closed position. The tube was then tilted to the most vertical position possible (about 60° for our apparatus). With the air bleed system on the raised end of the apparatus opened, the pump was turned on and the valve was opened to allow the fresh water to flow into the tilt tube. The tilt tube apparatus during the filling procedure is shown in Figure 3.

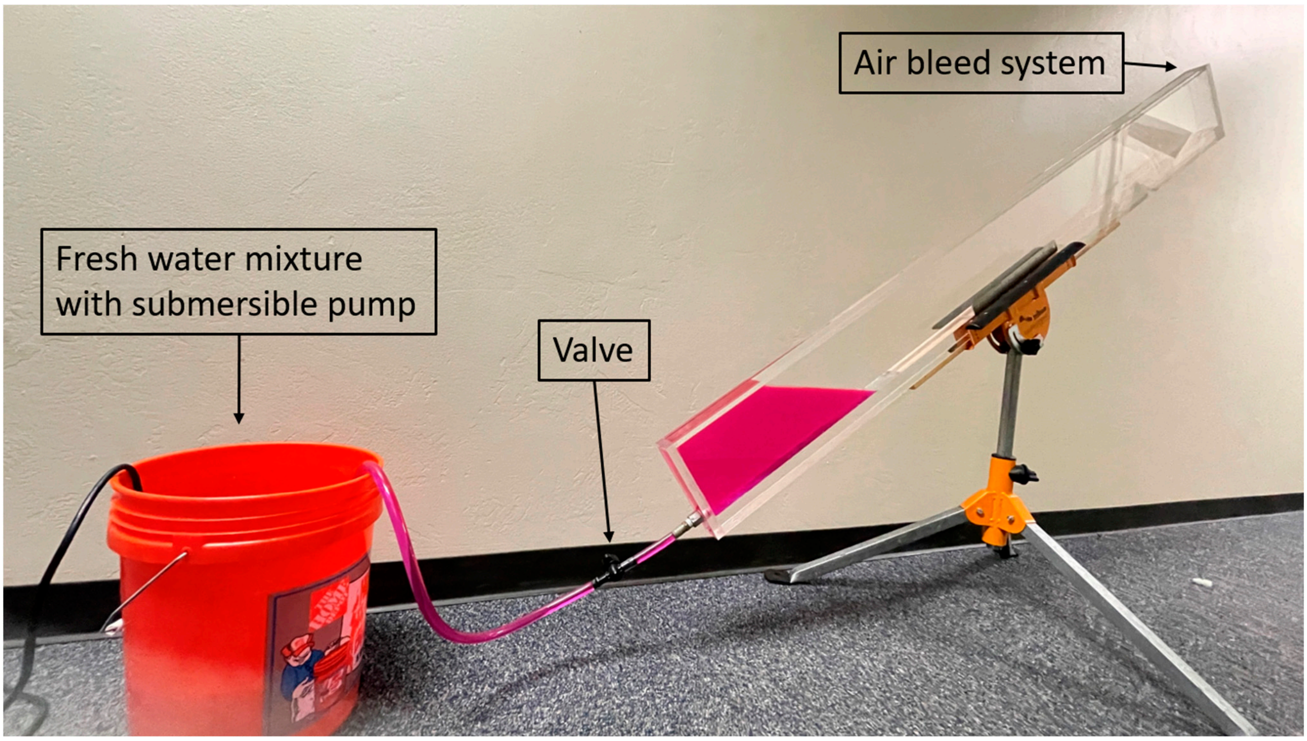

Figure 3. The tilt tube apparatus being filled with less dense fresh water.

The tilt tube was filled to the halfway point with the less dense fresh water. The valve was closed, and the plastic tubing was removed from the valve system. The process was repeated for the denser salt water, with the only difference being that the valve was opened minimally so that the salt water would be pumped into the tilt tube slowly enough to minimize mixing between the two fluids. Only after a substantial amount of salt water was introduced into the tilt tube could the valve be opened slightly more to increase the filling rate. The entire filling process took about 30 min, most of which was required for the salt water portion. After the tube was completely filled and the plastic tubing was removed from the valve system, the air bleed system was closed, and the apparatus was very slowly tilted until it was completely horizontal ($\theta = 0°$). As the tilting process created slight oscillations at the fluid interface, it was necessary to wait until they had died down to begin the experiment. The tilt tube setup before starting the experiment is shown in Figure 4. To promote the Kelvin-Helmholtz instability, a vertical perturbation was introduced by tilting the tube. The apparatus was quickly tilted from horizontal and was held in place by the bucket used to fill the tube (visible in Figure 4), such that the tilt angle was consistent from trial to trial. The tilt angle was determined through trial and error, and the goal was to ensure that the flow velocity was within the laminar flow regime. The tilt angle of this setup was 26°, which imparted a sufficient and consistent velocity in each volume to observe the waves while keeping the fluids in the laminar flow regime. This angle was chosen after preliminary tests showed that smaller angles did not produce large enough waves inside the tube. After the tank is tilted, buoyant forces accelerate the denser fluid toward the bottom of the tube and the lighter toward the top of the tube, which creates the velocity gradient across the interface necessary to induce the Kelvin-Helmholtz instability [17,18].

Figure 4. Filled tilt tube mounted on the Triton multi-stand in a horizontal position (θ = 0°). The fresh water is pink, and the denser salt water is blue.

Videos of the experiments were taken using a high-definition Nikon DSLR camera at a frame rate of 60 fps. The tilt tube was placed in front of an all-white backdrop to ensure that the waves were easily distinguishable, and a ruler was included in the frame to establish a length scale. Video stills were taken several times after the tube was tilted. The clearest visual evidence of the Kelvin-Helmholtz instability occurred 0.25–1 s after the tube was tilted. The stills were analyzed to determine the number and quality of the waves that formed.

2.4. CFD Model

Simulations of the Kelvin-Helmholtz instability were conducted using Ansys Fluent (version R2 2022), CFD software available to students via a free student edition. In this study, we investigated the behavior of the interface between two fluids within a tilted tube, utilizing the volume of fluid (VoF) method to accurately model the multiphase problem. An overview of the CFD modeling and solution steps are presented below. In-depth CFD tutorials can be found in [19].

2.4.1. Geometry

We created the geometry of the two-fluid system with an interface separating them. In Ansys Design Modeler, we created a 2D rectangular computational domain mirroring the cross-section of the experimental tilt tube. A 2D model of the tilt tube will reduce the complexity compared to a 3D model while capturing the complete physics of the system. The domain was 0.1524 m tall and 1.7653 m wide. To define the fluid region, we generated a rectangular sketch on the xy-plane, converted it to a surface body using the surface from the sketches tool, and designated it as fluid.

2.4.2. Mesh and Boundary Conditions

We generated a high-quality mesh to accurately capture the behavior of the instability. In the Ansys Mesh application, we initially inserted a face mesh with default settings to ensure the creation of quadrilateral elements. To control mesh density, we applied edge sizing to both the horizontal and vertical edges of the rectangle. The horizontal edges were divided into 4545 parts, while the vertical edges were divided into 450 parts, with adjustments made to account for the width/height difference to maintain aspect ratios near 1 [19]. Additionally, we changed the edge sizing behavior from 'soft' to 'hard'. This resulted in a mesh with 1,999,800 elements and 2,004,786 nodes. For ease of setup in Fluent, we used the edge selection filter to designate all four edges as 'Wall', which Fluent automatically assigned the wall boundary condition.

2.4.3. Multiphase Model

We used the multiphase model to simulate the interaction between the two fluids. In the Models tab, we activated the multiphase model, selecting the VoF option within the multiphase model box. The VoF model is commonly used for tracking the interface between two immiscible fluids. Default settings in the VoF model were used, with the Courant number set to 1 to satisfy the Courant-Friedrichs-Lewy (CFL) condition [19]. The primary phase was assigned as fresh water, and the secondary phase as salt water. Surface tension force modeling was enabled in the phase interactions tab, with a surface tension coefficient set to 0.00148 N/m [20]. Experimental work has shown that the surface tension is fairly insensitive to salt concentration [21], so this value was used in all simulations. We conducted an additional simulation with surface tension adjusted for the high salinity case (0.00296 N/m) and confirmed that the surface tension had no impact on the results.

2.4.4. Solver Settings

We adopted a pressure-based solver with an absolute velocity formulation for a transient 2D planar simulation. To account for the tilt angle of 26°, we activated gravity, setting the x- and y-components to $-4.3004\ \mathrm{m/s^2}$ and $-8.8172\ \mathrm{m/s^2}$, respectively. The material properties, essential for the multiphase model, were defined with densities of $998.2\ \mathrm{kg/m^3}$ and $1079.2\ \mathrm{kg/m^3}$, and dynamic viscosities of $0.001002\ \mathrm{kg/m{\cdot}s}$ and $0.0012\ \mathrm{kg/m{\cdot}s}$ for fresh water and salt water, respectively, based on the parameters for Trial 1 [22]. We performed three additional trials by varying the density and the viscosity (i.e., the salinity) to match the experimental values listed in Table 1. The laminar solver was used, and solution methods were configured with the SIMPLE method. The momentum equation was set to second-order upwind for improved accuracy. To ensure model convergence, we set residual targets to 10^{-4}. We ran transient simulations to capture the dynamic evolution of the instability.

2.4.5. Initialization

To initialize the simulation with the lower portion of the geometry representing salt water, a mesh adaptation is required. We accessed the "Manual Mesh Adaptation" feature, selected "Cell Registers", and created a "New Region". We specified the spatial coordinates (0, 0) and (1.7653, 0.7620), which define the boundaries of the lower half of the rectangular domain.

Next, we proceeded to the standard initialization process by clicking "Initialize" and subsequently selecting "Patch". Within the newly defined region, we changed the phase to salt water and set the volume fraction to 1. Afterward, we reverted the phase back to a mixture and set the x-velocity within the designated region to be 0 m/s.

2.4.6. Visualization and Data Generation

Phase contour graphics played a pivotal role in visualizing the progression of the Kelvin-Helmholtz instability. To create a phase contour, we initiated the simulation, patched the salt water phase to a value of 1 in the lower region, and subsequently adjusted the horizontal velocity to zero for the mixture. This sequence of actions allowed us to generate a fresh water phase contour, providing profound insights into the dynamics of the instability. Additionally, it served as a crucial step in validating the simulation's initialization and setup.

We created a solution animation that produced JPEG images of the phase contour every 0.01 s. These images are located in the project files upon the completion of the simulation, enabling a detailed record of the instability's evolution [15].

2.4.7. Calculation

We implemented multiphase-specific adaptive time stepping to calculate an optimal time step based on the target Courant number and precision settings, ensuring efficiency and accuracy. Each simulation ran to a total time of 2.5 s, with a Courant number of 1 to again satisfy the CFL condition, and 1000 iterations per timestep were allowed to ensure each time step converged properly. We started the simulation and monitored the convergence by making adjustments as necessary to ensure accurate results.

A mesh sensitivity study was performed. The mesh was refined several times, and we compared the results obtained with the refined meshes to those from the initial mesh. We looked for changes in wave amplitude and wavelengths to assess whether the results were converging. We continued refining the mesh until the results were unchanged. The wavelength and wave amplitude remained nearly constant when the mesh density was increased from a little over 2 million to 3 million nodes; therefore, we used the mesh with 2 million nodes for the study. It is worth noting that once surface tension at the interface is included, mesh sensitivity is hard to assess [23].

To expedite computations, the final simulations were executed on our university's high-performance computer. We utilized one node (of sixteen) that has two CPUs, sixteen 2.5 GHz Intel Xeon cores, and 64 GB of RAM. With a mesh comprising approximately two million elements, the first two trials ran for about 14 h while the third and fourth trials ran for over 24 h. On a desktop Dell Precision 3450 with four 11th Gen Intel 2.5 GHz processors and 16 GB of RAM, Trial 1 took almost four days to complete. For faster results in a classroom setting, a coarser mesh can be employed to reduce run time.

2.5. Comparison of Experimental and Numerical Results

A quantitative comparison of the experimental results with the CFD results was carried out by measuring the number and mean amplitude of the waves in each trial. Stills from both the videos and simulations were evaluated with Digimizer (version 6.3), which is a free image analysis software package [24]. For each image, a reference dimension (the length of the tube in the simulation images and the ruler in the experiment images) was chosen, and then each discernable wave formation was measured from top to trough to determine the amplitude of each. The software then calculated an accurate measurement based on the reference dimension and outputs the number of waves and mean amplitude.

3. Results

3.1. Experimental Results

Video stills taken from the four trials are shown in Figures 5–8. In each trial, t = 0 s was defined as the last frame in the video before there was visual evidence of wave development.

Video stills were then taken every 10 frames (1/6 s), and the four stills shown below represent the best views of the wave development for each trial over the course of the experiment, which was recorded for about 2 s total. In the case of Trial 1 (Figure 5), the instability developed later than in the other three trials, with substantial wave development occurring about half a second after the tube was tilted. At the lowest salinity level (7.5%), there was initially a smaller number of waves that were more centrally located along the length of the tube than in the other three cases. The wave amplitude also initially varied, with the largest amplitudes occurring near the central location, decreasing at further distances from the center. This corresponded to a slight delay in wave development at further distances from the center, meaning that the central waves had already crested and mixed as the waves further from the center were still crisp.

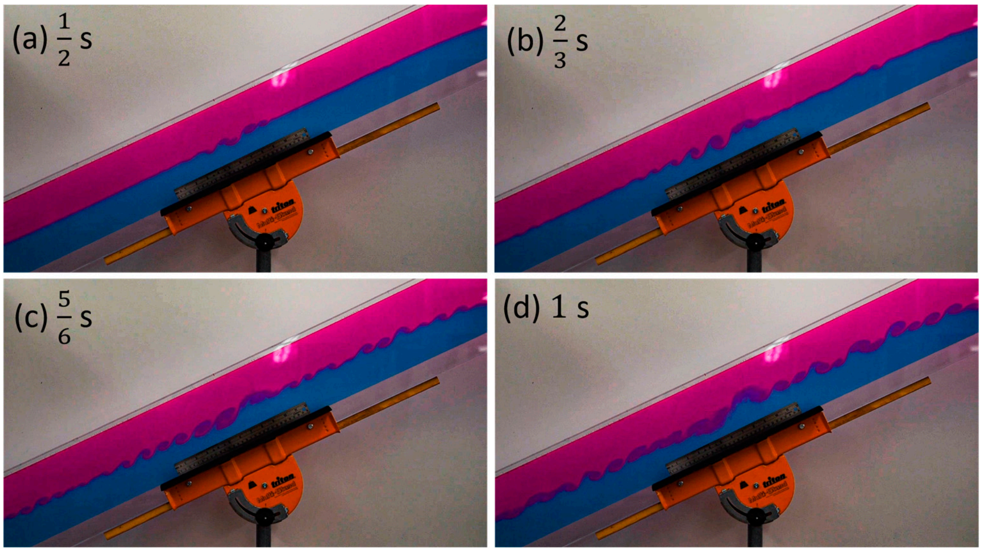

Figure 5. Video stills of Trial 1, which had a salt water salinity of 7.5%. The time noted on each still is the time after the first visual evidence of wave development was observed.

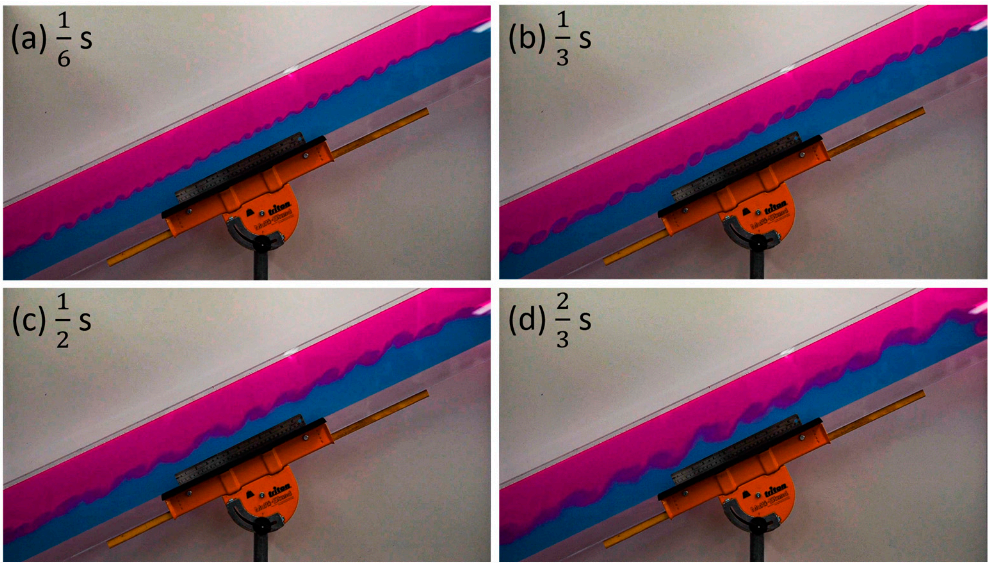

Figure 6. Video stills of Trial 2, which had a salt water salinity of 11.5%. The time noted on each still is the time after the first visual evidence of wave development was observed.

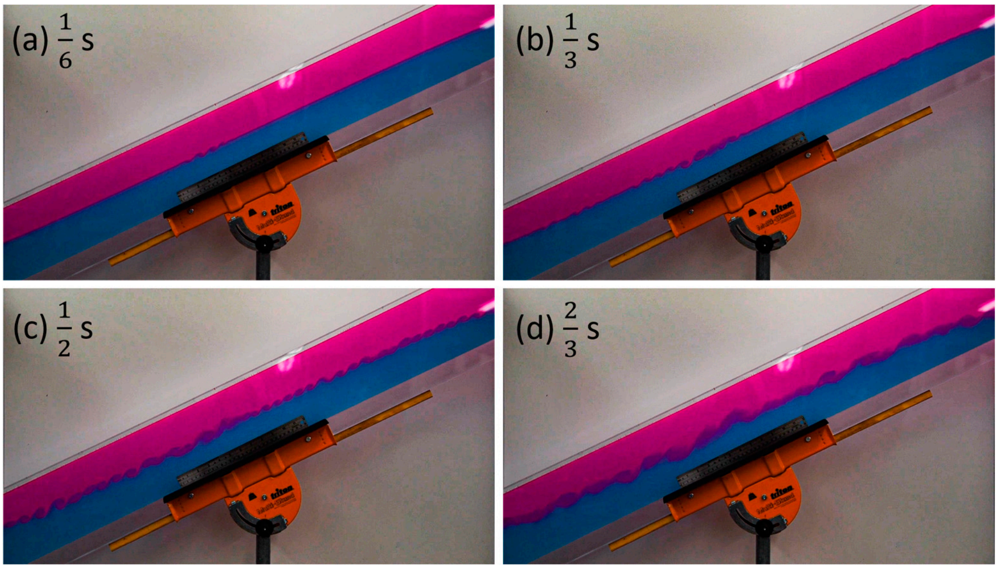

Figure 7. Video stills of Trial 3, which had a salt water salinity of 15.5%. The time noted on each still is the time after the first visual evidence of wave development was observed.

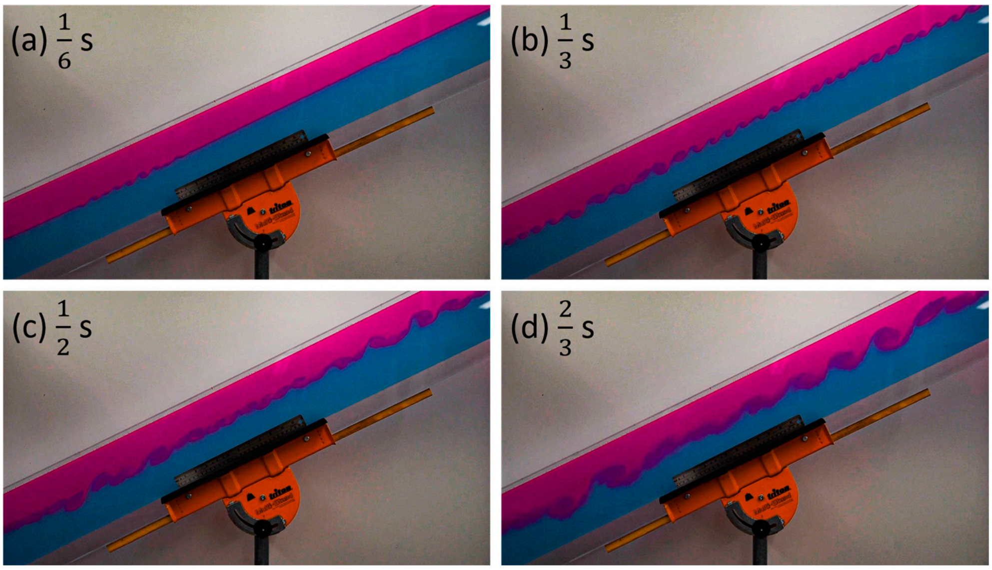

Figure 8. Video stills of Trial 4, which had a salt water salinity of 19.5%. The time noted on each still is the time after the first visual evidence of wave development was observed.

While the other three cases also exhibited wave development centrally, at a salinity level of 11.5% (Figure 6), the instability developed so quickly that at the first still, the waves were already developed and appeared uniformly across the length of the tube. A larger difference in density between the two fluids will result in a more pronounced displacement and often leads to a higher growth rate of the instability. This means that the perturbations at the interface grow more rapidly, resulting in a larger displacement over a given period of time. In regard to wavelength, an increased density contrast can lead to shorter wavelength structures and finer features in the evolving interface.

3.2. CFD Results

We extracted data and visualized the development of the Kelvin-Helmholtz instability, including the displacement of the interface and the formation of vortical structures. Contour plots and animations to study the behavior of the instability in detail were created in post-processing. The Kelvin-Helmholtz instability is captured in Figures 9–12 for Trials 1–4, respectively, providing a comprehensive depiction of the wave development. Images capturing the interface at t = 1 s, 1.5 s, 2 s, and 2.5 s are presented for Trials 1 and 2, while images capturing the interface at t = 0.5 s, 1 s, 1.5 s, and 2 s are presented for Trials 3 and 4 since the larger difference in density between the two fluids in Trials 3 and 4 caused the perturbations at the interface to grow much faster.

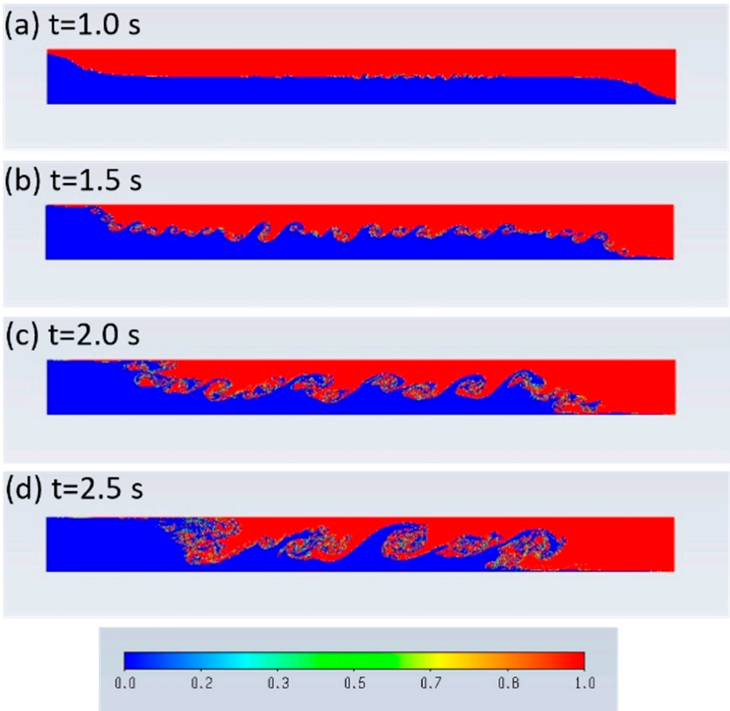

Figure 9. Contours of Trial 1, which was simulated with a salt water salinity of 7.5%.

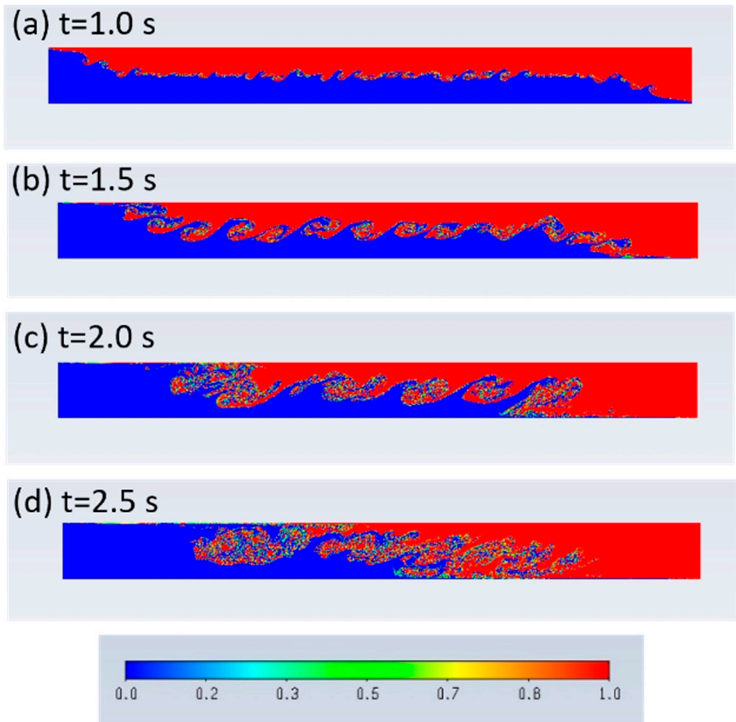

Figure 10. Contours of Trial 2, which was simulated with a salt water salinity of 11.5%.

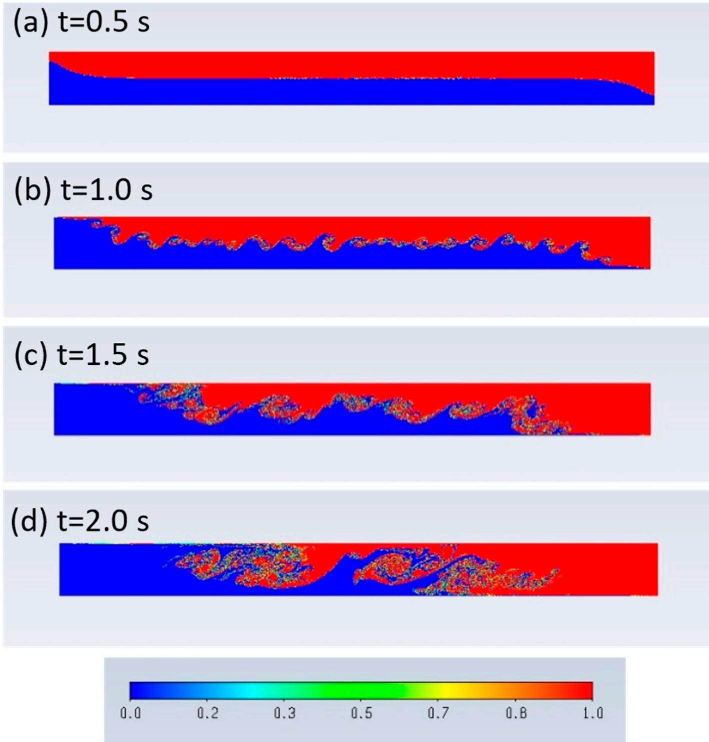

Figure 11. Contours of Trial 3, which was simulated with a salt water salinity of 15.5%.

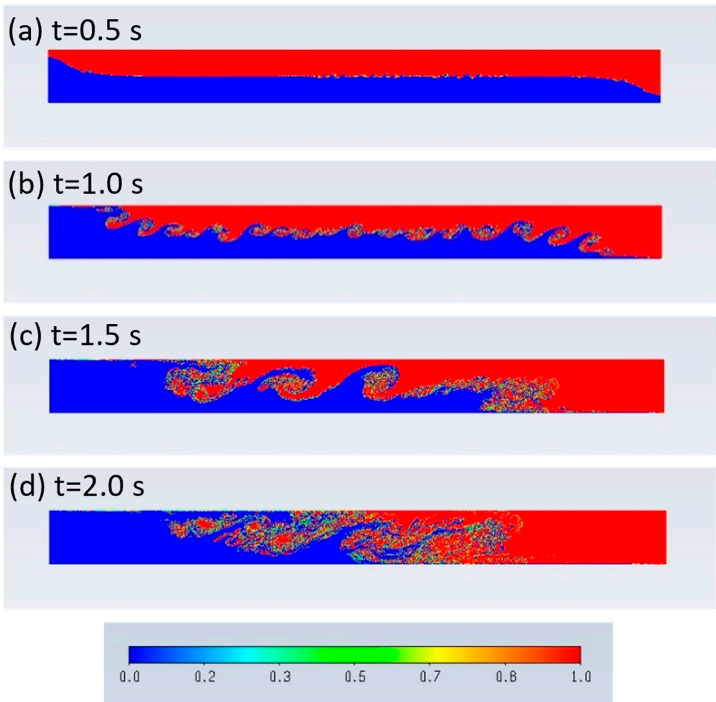

Figure 12. Contours of Trial 4, which was simulated with a salt water salinity of 19.5%.

In the first image for all trials, the interface between the two fluids exhibits subtle undulations. As time progresses, the undulations intensify, leading to the formation of well-defined vortices and waves in the second and third images. Notably, by the time we reach the fourth and final image in the sequence, the two fluid layers start to mix and become fully turbulent, marking the point of complete intermingling between the two fluids.

These images offer valuable insights into the dynamic evolution of the Kelvin-Helmholtz instability and its eventual transition to a state of complete mixing.

3.3. Comparison of Numerical and Experimental Results

Video stills taken at t = 1 s from the four experimental trials are shown in Figure 13, and the interface contours observed in the CFD simulations at t = 1.5 s for all four trials are shown in Figure 14. The actual difference between the timing of the beginning of the experiment and the modified t = 0 s used to identify the video stills above was approximately 0.5 s; this accounts for the small but quantifiable delay in the tilting process itself. Qualitatively, there are significant differences in the development of the interface between scenarios with varying salinity levels that are captured in both the experiments and simulations. Higher salt water density conditions tend to result in fewer waves being formed at the interface. In addition, the greater density difference leads to stronger velocity gradients and shear at the interface. This increased shear generates more vortices, causing larger displacements and more pronounced interfacial deformations.

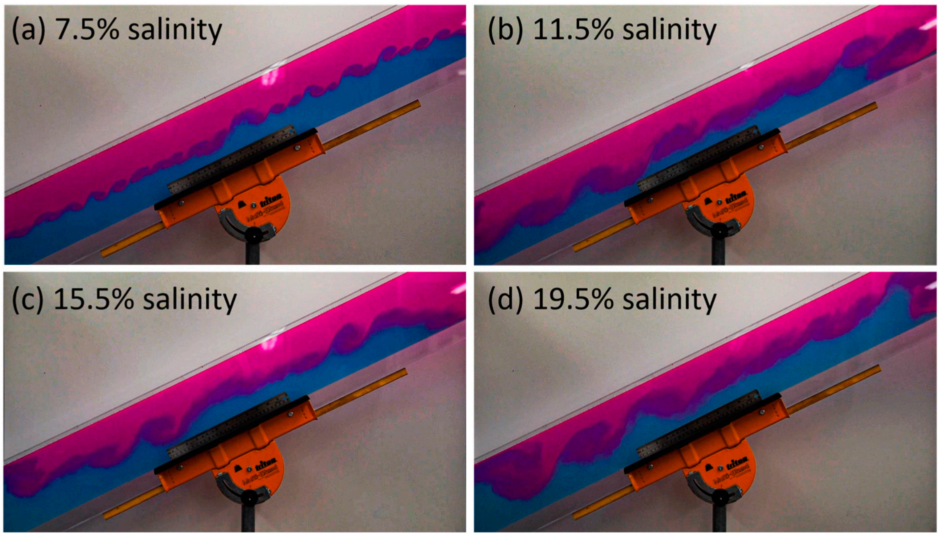

Figure 13. Video stills of all four experimental trials at t = 1 s.

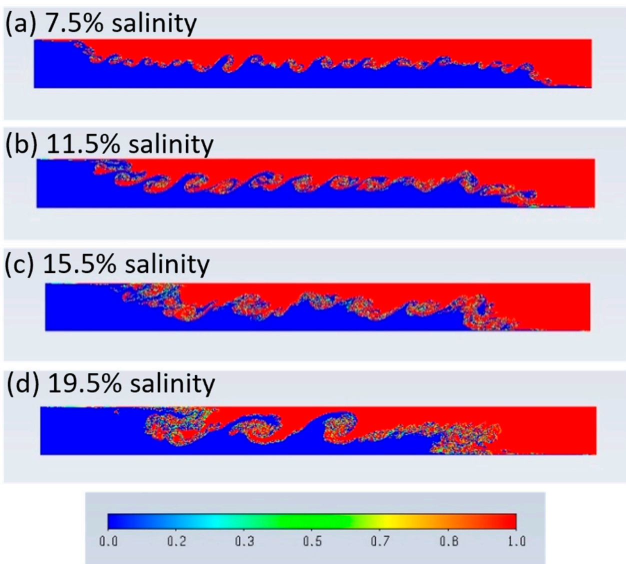

Figure 14. Contours of all four CFD trials at t = 1.5 s.

The results of the image analysis of the experimental video stills and the numerical interface contours are shown in Figure 15. Figure 15a shows the mean wave amplitude as a function of salinity for both experimental and CFD simulation trials. The x-axis represents varying salinity levels, while the y-axis corresponds to the mean amplitude of the waves. The mean wave amplitude increases with higher salinity levels for both experimental and simulated conditions. Figure 15b shows the number of waves generated in the tilt tube as a function of salinity for both experimental and CFD simulation trials. Similar to Figure 15a, the x-axis represents different salinity levels, while the y-axis is the number of waves produced. In both experimental and simulated data, the number of waves generated in the tilt tube is shown to be decreasing as the salinity increases.

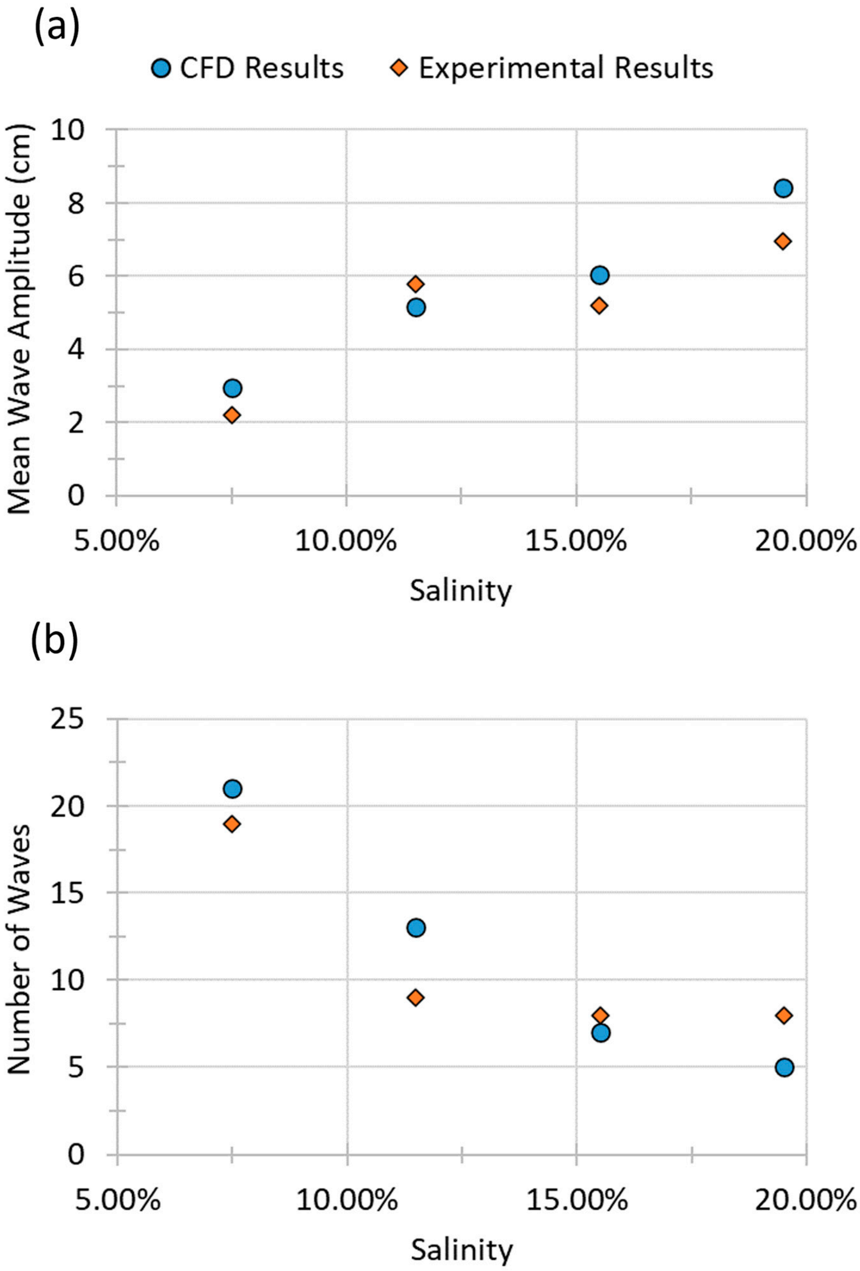

Figure 15. Image analysis results of experimental video stills and numerical interface contours for all four trials show (**a**) the mean wave amplitude as a function of salinity and (**b**) the number of waves as a function of salinity.

4. Discussion

The primary goals of this work were to detail the development of a low-cost tilt tube apparatus that could be used to augment the basic experiments in a thermal-fluids laboratory course to allow students to induce and record the Kelvin-Helmholtz instability, and the development of a 2D CFD model that could allow students to numerically simulate the instability and validate their CFD models. In both the experiments and the CFD simulations, students can determine the effects of changing the salt water fluid density on the waves that form in the ensuing Kelvin-Helmholtz instability. As the kinematic viscosity of a fluid depends on its density, a density change will alter how that fluid responds to forces imparted on it.

The experimental procedure is fairly straightforward, and fourth-year engineering students should have no issues setting up and running the experiment. Currently, this is the only experiment in either of the required laboratory courses (mechanics of materials is the other required laboratory course) that utilizes video recording and analysis. A secondary benefit of the experiment is that the recorded data can be provided to students in the introductory CFD course to allow them to validate their model after they have numerically simulated the Kelvin-Helmholtz instability. Developing a 2D CFD model with two different fluid types in Ansys Fluent is well within their capabilities after completing initial software and simulation tutorial exercises and homework.

Utilizing experimental data to validate CFD models constitutes a crucial step in verifying the reliability of numerical techniques. Although the Fluent model of the tilt tube experiment indicated functionality, it is worth noting that the current paper's focus and objectives did not encompass formal model validation. For future research, we propose selecting a specific salinity experiment from the dataset and conducting a rigorous validation of the numerical model.

5. Conclusions

In summary, this paper introduced an experimental apparatus and corresponding CFD model to investigate the Kelvin-Helmholtz instability, a phenomenon arising from the interaction between fluids with varying densities. The low-cost tilt tube apparatus facilitated the observation and recording of the instability, offering a practical platform for exploring fluid mechanics concepts. The study demonstrated the successful implementation of a 2D CFD model using Ansys Fluent to simulate the Kelvin-Helmholtz instability within the tilt tube. The numerical simulations captured the multiphase flow and instability dynamics. The emphasis on varying salt water salinity in both experiments and simulations provided insights into the effects of salinity changes on the evolving Kelvin-Helmholtz instability. The broader significance of this study is to advance our understanding of multiphase flow behavior and fluid instability. The integration of experimental and numerical approaches offers a comprehensive perspective on the Kelvin-Helmholtz instability and its sensitivity to salinity variations. Future research could delve deeper into fluid interactions and refine the CFD model for more accurate predictions of fluid instability phenomena.

Author Contributions: Conceptualization, I.K.; Methodology, I.K.; Validation, M.M.G., D.M. and I.K.; Formal analysis, M.M.G., D.M. and I.K.; Investigation, M.M.G., D.M. and I.K.; Resources, I.K.; Data curation, M.M.G. and I.K.; Writing—original draft, M.M.G., D.M. and I.K.; Writing—review & editing, M.M.G., D.M. and I.K.; Visualization, M.M.G., D.M. and I.K.; Supervision, M.M.G. and I.K.; Project administration, I.K. All authors have read and agreed to the published version of the manuscript.

Funding: This research received no external funding.

Data Availability Statement: The experimental data presented in this study are openly available in FigShare [25]. The CFD data presented in this study are available on request from the corresponding author. The data are not publicly available due to the size of the files.

Conflicts of Interest: The authors declare no conflict of interest.

References

1. Helmholtz, H.V. On Discontinuous Movements of Fluids. *Lond. Edinb. Dublin Philos. Mag. J. Sci.* **1868**, *36*, 337–346. [CrossRef]
2. Thomson, W. (Lord K.). Hydrokinetic Solutions and Observations. *Lond. Edinb. Dublin Philos. Mag. J. Sci.* **1871**, *42*, 362–377. [CrossRef]
3. Thomson, W. (Lord K.). On the Stability of Steady and of Periodic Fluid Motion. *Lond. Edinb. Dublin Philos. Mag. J. Sci.* **1887**, *23*, 459–464. [CrossRef]
4. Ellrod, G.P.; Knox, J.A.; Lester, P.F.; Ehernberger, L.J. Aviation Meteorology: Clear Air Turbulence. In *Encyclopedia of Atmospheric Sciences*, 2nd ed.; Elsevier: Amsterdam, The Netherlands, 2014. [CrossRef]
5. Luce, H.; Nishi, N.; Caccia, J.L.; Fukao, S.; Yamamoto, M.K.; Mega, T.; Hashiguchi, H.; Tajiri, T.; Nakazato, M. Kelvin-Helmholtz Billows Generated at a Cirrus Cloud Base within a Tropopause Fold/Upper-Level Frontal System. *Geophys. Res. Lett.* **2012**, *39*, L04807. [CrossRef]
6. Smyth, W.D.; Moum, J.N. Ocean Mixing by Kelvin-Helmholtz Instability. *Oceanography* **2012**, *25*, 140–149. [CrossRef]
7. Matza, M. Kelvin-Helmholtz: Rare Wave Clouds Amaze Sky-Watchers in Wyoming. BBC News. Available online: https://www.bbc.com/news/world-us-canada-63912257 (accessed on 4 May 2023).
8. Armengol, S.; Raush, G.; Gamez-Montero, P.J. In-House Low-Cost Water Table Prototype to Practically Analyse the Modelling Compressible Flow in a Fluid Engineering Course. *Int. J. Mech. Eng. Educ.* **2022**, *50*, 990–1006. [CrossRef]
9. Goushcha, O.; Angira, S. Classroom Demonstration of a Stagnation Flow Using Cell Phone-Captured Particle Image Velocimetry Data. *Int. J. Mech. Eng. Educ.* **2022**, *50*, 978–989. [CrossRef]
10. Faisal, S.H. Design, Fabrication, and Testing of Heat Conduction Apparatuses at a Low Cost. *Int. J. Mech. Eng. Educ.* **2023**, *51*, 89–110. [CrossRef]
11. Severo Foresto, J.P.; Martins, W.S.; do Lago, T.G.S.; da Silva Marques, A. Development of a Low-Cost Data Acquisition System for a Vapor Compression Refrigeration Experimental Workbench. *Int. J. Mech. Eng. Educ.* **2023**, *51*, 194–208. [CrossRef]
12. Mokhtar, W. Using Computational Fluid Dynamics to Introduce Critical Thinking and Creativity in an Undergraduate Engineering Course. *Int. J. Learn.* **2010**, *17*, 441–458. [CrossRef]
13. Zamora, B.; Kaisera, A.S.; Vicente, P.G. Improvement in Learning on Fluid Mechanics and Heat Transfer Courses Using Computational Fluid Dynamics. *Int. J. Mech. Eng. Educ.* **2010**, *38*, 147–166. [CrossRef]
14. Jithish, K.S.; Ajay Kumar, P.V. Analysis of Turbulent Flow through an Orifice Meter Using Experimental and Computational Fluid Dynamics Simulation Approach—A Case Study. *Int. J. Mech. Eng. Educ.* **2015**, *43*, 233–246. [CrossRef]
15. FLUENT. *Ansys Fluent User Guide 2022R2*; ANSYS Inc.: Canonsburg, PA, USA, 2022.
16. SOLIDWORKS. *Introducing SolidWorks*; SolidWorks Corporation: Concord, MA, USA, 2023.
17. De Silva, I.P.D.; Fernando, H.J.S.; Eaton, F.; Hebert, D. Evolution of Kelvin-Helmholtz Billows in Nature and Laboratory. *Earth Planet. Sci. Lett.* **1996**, *143*, 217–231. [CrossRef]
18. Thorpe, S.A. Experiments on the Instability of Stratified Shear Flows: Miscible Fluids. *J. Fluid Mech.* **1971**, *46*, 299–319. [CrossRef]
19. Khalil, I.; Lakkis, I. *Computational Fluid Dynamics: An Introduction to Modeling and Applications*, 1st ed.; McGraw Hill Professional: New York, NY, USA, 2023.
20. Alterman, Z. Effect of surface tension on the kelvin-helmholtz instability of two rotating fluids. *Proc. Natl. Acad. Sci. USA* **1961**, *47*, 224–227. [CrossRef] [PubMed]
21. Hauner, I.M.; Deblais, A.; Beattie, J.K.; Kellay, H.; Bonn, D. The Dynamic Surface Tension of Water. *J. Phys. Chem. Lett.* **2017**, *8*, 1599–1603. [CrossRef] [PubMed]
22. Sharqawy, M.H.; Lienhard, J.H., V; Zubair, S.M. Thermophysical Properties of Seawater: A Review of Existing Correlations and Data. *Desalin. Water Treat.* **2010**, *16*, 354–380. [CrossRef]
23. Štrubelj, L.; Tiselj, I. CFD Simulation of Kelvin-Helmholtz Instability. In Proceedings of the Nuclear Energy for New Europe, Bled, Slovenia, 5 September 2005.
24. Digimizer Image Analysis Software. Available online: https://www.digimizer.com (accessed on 4 December 2023).
25. Experimental Kelvin-Helmholtz Results—Gibbons, Muldoon, and Khalil. 2023. Available online: https://figshare.com/articles/dataset/dx_doi_org_10_6084_m9_figshare_24790656/24790656 (accessed on 11 December 2023).